MAGNETOHYDRODYNAMICS Vol. 51 (2015), No. 2, pp. 267–274

MAGNETIC FIELD IN A DECAYING SPIN-DOWN FLOW OF LIQUID SODIUM

P. Frick[1], *S. Denisov*[1], *V. Noskov*[1], *A. Pavlinov*[1], *R. Stepanov*[1,2]

[1] *Institute of Continuous Media Mechanics, 1 Acad.Korolyov str., Perm 614013, Russia*
[2] *State National Research Polytechnical University of Perm, 29 Komsomolskii ave., 614990 Perm, Russia*

The expulsion of magnetic field by strong turbulence is studied experimentally in a non-stationary turbulent flow of liquid sodium generated in a toroidal channel at a moderate magnetic Reynolds number Rm > 10. The applied toroidal magnetic field is mainly collinear with the streamline of a large-scale flow, which reduces the induction effects caused by the mean flow and makes it possible to isolate the contribution of turbulent effects. It is shown that at the highly turbulent stage of flow evolution the mean magnetic field along the channel axis decreases by 30%. The observed effect can be explained as the result of turbulent diamagnetism described by the term $\boldsymbol{\gamma}\boldsymbol{\nabla} \times (\mathbf{g} \times \mathbf{B})$ of the mean field induction equation, where $\mathbf{g}$ is the normalized gradient of the energy of turbulent fluctuations and $\mathbf{B}$ is the mean magnetic field.

Introduction. Intensive small-scale turbulence in electroconducting fluids gives rise to a variety of induction effects described by about 20 terms in the general expression of mean electromotive force [1]. Only few of them have been studied in details. For laboratory study, the generation of the MHD configuration, which allows isolation of contributions of different effects, is a hard problem [2]. In our paper, we present the results of laboratory measurements of magnetic field variations in a domain affected by strong turbulent fluctuations. A series of experiments with a nonstationary turbulent flow of liquid sodium generated in a fast rotating toroidal channel after its abrupt braking is performed. The applied stationary toroidal magnetic field is mainly collinear with the streamline of the large-scale mean flow, namely, with the toroidal flow, which is an order of magnitude stronger than the poloidal one. This reduces the induction effects caused by the mean flow and makes it possible to separate the contribution of turbulence.

1. Experimental setup. We study a spin-down flow of liquid sodium in a toroidal channel made of titanium alloy [3]. The torus has the radius $R = 0.18$ m and the radius of the channel cross-section $r_0 = 0.08$ m. The rotation frequency of the channel Ω is up to 50 rps and the flow in the channel is generated by abrupt braking. The braking time does not exceed 0.3 s. After the channel has come to a full stop, the velocity of the sodium flow is about 70% of the linear velocity before braking. This means that the Reynolds number $\mathrm{Re} = V r_0/\nu$ reaches $\mathrm{Re} \approx 3 \cdot 10^6$ at the most, which corresponds to the magnetic Reynolds number $\mathrm{Rm} \approx 30$.

For velocity measurements, a 2-axis local probe was used designed to ensure good dynamical resolution of toroidal and poloidal motions in liquid metals [4]. The probe was mounted on the channel wall in such a way that it stuck out inside the channel by 1.5 mm so that the measurements were made away from the boundary layers for any phase of the non-stationary flow evolution. At the first stage of braking, the toroidal velocity of the fluid with respect to the halting vessel increases (as the probe is attached to the vessel). The measurements were made in this initially moving frame of reference, and the initial zero value of the fluid velocity corresponded to solid body rotation. The maximum of the toroidal velocity

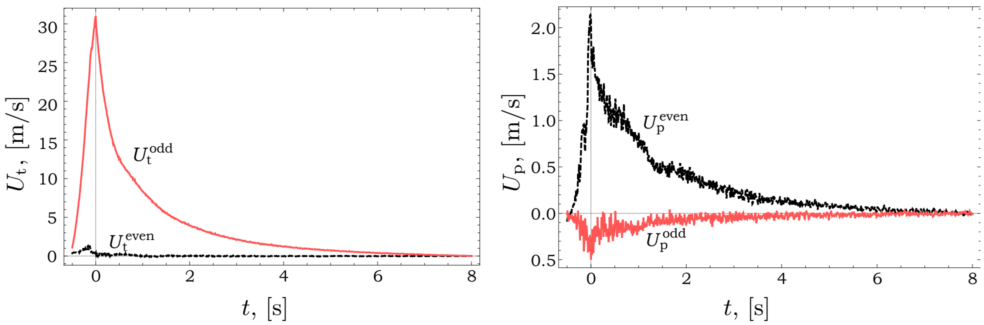

Fig. 1. Evolution of mean toroidal (left) and poloidal (right) velocities for $\Omega = 40$ rps. The black dashed line corresponds to the even part of signals (half-sum of signals obtained for the opposite direction of channel rotation), and the red solid line is the odd (half-difference) part of signals.

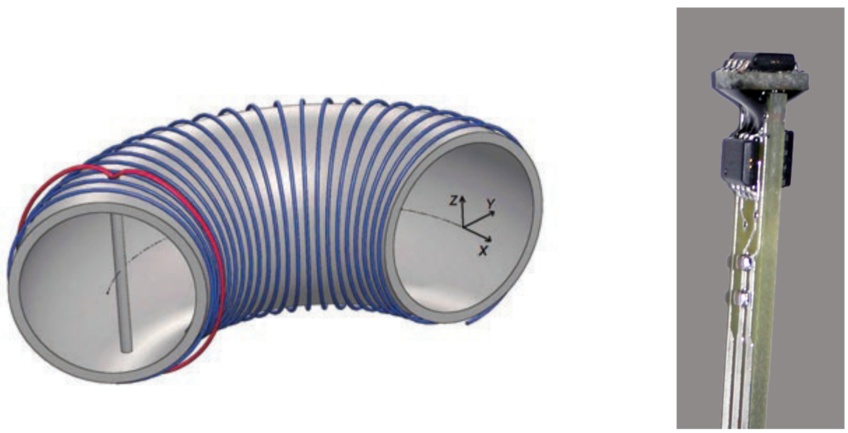

(*a*) (*b*)

Fig. 2. (*a*) Scheme of the toroidal channel and coils, (*b*) 3-component magnetic field probe.

was reached when the vessel came to a full stop, and the subsequent dynamics was measured in the frame at rest. At this stage, the transverse (poloidal) velocity developed. The corresponding variations of the toroidal and poloidal velocities averaged over 20 runs are shown in Fig. 1, where $t = 0$ corresponds to the end of braking. We plot the even and odd parts of the velocity components (the half-sum and the half-difference of values obtained for clockwise and counterclockwise channel rotations) to show that the sign of toroidal mode depends on the rotation direction and the sign of poloidal mode does not. The generation of poloidal velocity is feasible in the curved channel and becomes more effective with the increasing "thickness" of the torus [5]. For the maximal rotation rate $\Omega = 50$ rps, at the end of braking, the ratio of poloidal to toroidal mean velocities reaches $U_{\rm p}/U_{\rm t} = 0.18$. The maximum toroidal velocity $U_{\rm t} = 0.69V_0 = 39$ m/s, where V_0 is the velocity of the sodium on the channel axis before the brake. The evolution of this nonstationary spin-down flow is described in detail in [4].

The applied magnetic field is generated by a toroidal coil, which is wound around the channel (60 turns). This coil (shown in Fig. 2*a*) is fed by a stabilized direct current $I \approx 20$ A and produces a toroidal field $B_0(y)$ with induction $\simeq 13$ Gs at the axis of the channel. A tube of 10 mm diameter crosses the channel parallel to the axis of rotation (Fig. 2*a*) and is located at the channel cross-section opposite the velocity probe. This tube can be used both for local and for integral magnetic field measurements. Three components of the local magnetic field are measured by the 3D Hall probe (see Fig. 2*b*) based on Sentron's CSA-1VG chips with 28 mV/Gs magnetic sensitivity. The probe can be fixed at any position along the tube defined by the coordinate z.

The same tube was used for magnetic flux measurements by special coils, each enveloping one half of channel's cross-section (shown in red in Fig. 2*a*). The signals from the coils are amplified by a low noise voltage preamplifier SR560 and allow us to control the variation of the magnetic flux in each half of the cross-section. To control the variation of the total magnetic flux, an additional coil was used, which was wound around the entire body of the channel in parallel to the power coil. Before passing the sliding contacts, the signal from this coil is amplified by a preamplifier K140UD17A mounted on the axis of torus rotation.

2. Induced magnetic field. The applied magnetic field B_0 is homogeneous along the measuring tube and equal to about 13 Gs. We measured the magnetic field at different positions of the probe in the channel. The coordinate z shows the position of the probe in the tube: $z = 0$ corresponds to the central position in the torus cross-section, $z = \pm 80$ mm are the left and right extreme positions in the tube. The mean value of the *induced* magnetic field B (the applied field is subtracted) is calculated by averaging over 10 realizations and taking the moving averaged over the 0.01 s window. The difference between the actual measured magnetic field and the mean value B gives the estimate of the fluctuating part of magnetic field b. Fig. 3 shows the smoothed evolution of the two components B_x and B_z. The upper panels in Fig. 3 show the even part of the magnetic field (half-sum of signals obtained for both directions of the channel rotation), and the lower panels show the odd component with respect to the direction of rotation (half-difference).

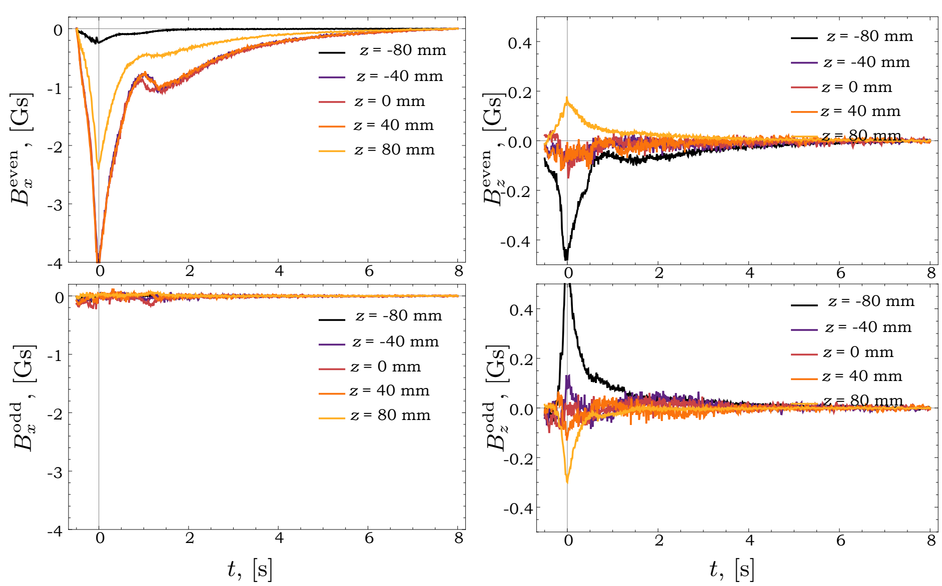

Fig. 3. Evolution of the mean induced magnetic field in several positions along the z-axis. The upper panels correspond to the half-sum (even part) and the lowers to the half-difference (odd part) of B measurements obtained for clockwise and counterclockwise rotations of the torus.

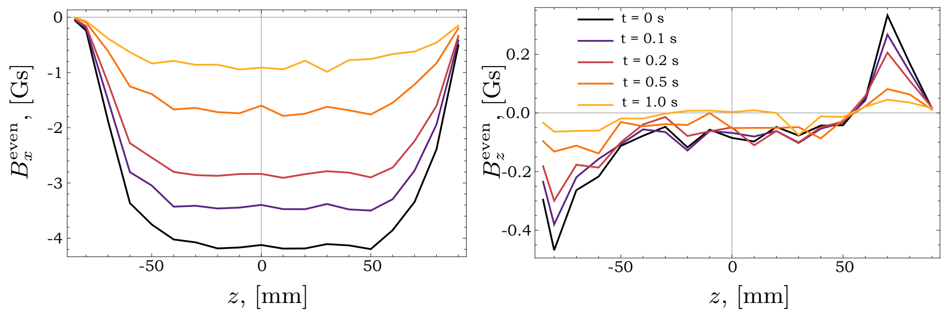

Fig. 4. Profiles of induced magnetic field components at several time points.

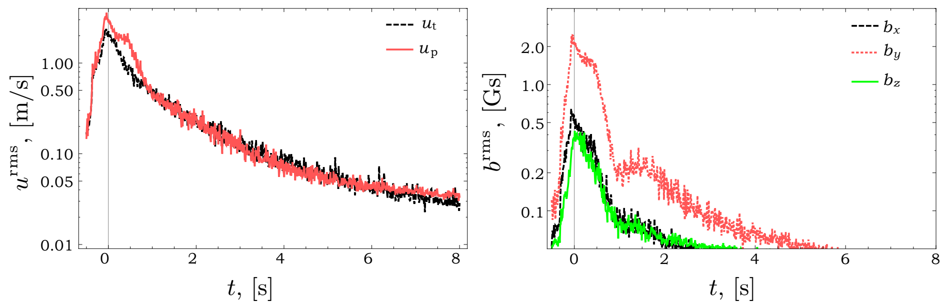

Fig. 5. R.m.s. pulsations of toroidal and poloidal velocity components (left) and r.m.s. pulsations of induced magnetic field components (right).

The effect of magnetic field suppression in the turbulent flow core is clearly seen in the toroidal component. The induced field B_x reaches about -4 Gs in the end of breaking, when the intensity of the turbulent flow is maximum (minus means that the induced field is opposite to the applied field). The effect is strictly even with respect to the direction of rotation, notably the applied field decreases for any direction of the flow. This field suppression can be attributed to the expulsion of the magnetic field from the turbulent core to the outer part of the channel cross-section, however, the contribution of other mechanisms, e.g., the simple drift provided by the flow around the tube, should be excluded. Similar reduction of the external magnetic field by turbulence was observed in the Riga dynamo experiment [6]. It was interpreted as a skin effect.

The induced field B_z is essentially weaker (below 0.5 Gs) and includes both the even and the odd modes (Fig. 3, right). The component B_z is mainly concentrated near the wall and apparently is caused by a drift of inhomogeneities of the applied magnetic field occurring due to the large distance between the coil turns (13 mm).

Fig. 4 presents a distribution of the induced magnetic field along the z-axis in the cross-section of the torus at different stages of flow decay. The profile of the induced toroidal component B_x supports the basic idea that the effect of magnetic field displacement is caused by the intense turbulent flow – the profile is flat in the domain of the turbulent core and decreases in the vicinity of the walls. On the contrary, the induced B_z component is concentrated near the walls and orientated in the opposite direction. Fig. 5 shows how the r.m.s. pulsations of velocity and magnetic field components evolve and decay.

During the first second of the flow decay, turbulence is strongly anisotropic – the plot illustrates the dominance of poloidal velocity pulsations at this stage. The right panel of Fig. 5 shows that the r.m.s. pulsation of the magnetic field follows the r.m.s. pulsation of the poloidal velocity. Note that the magnetic

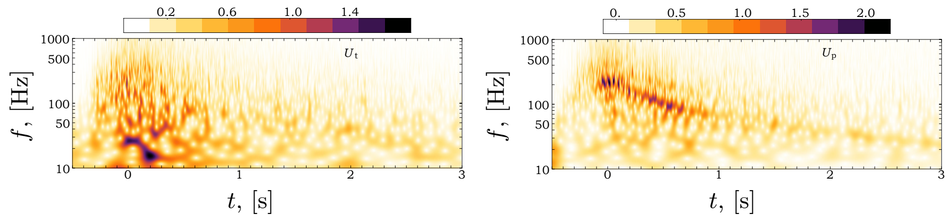

Fig. 6. Wavelet spectrograms of U_t (left) and U_p (right) fluctuations.

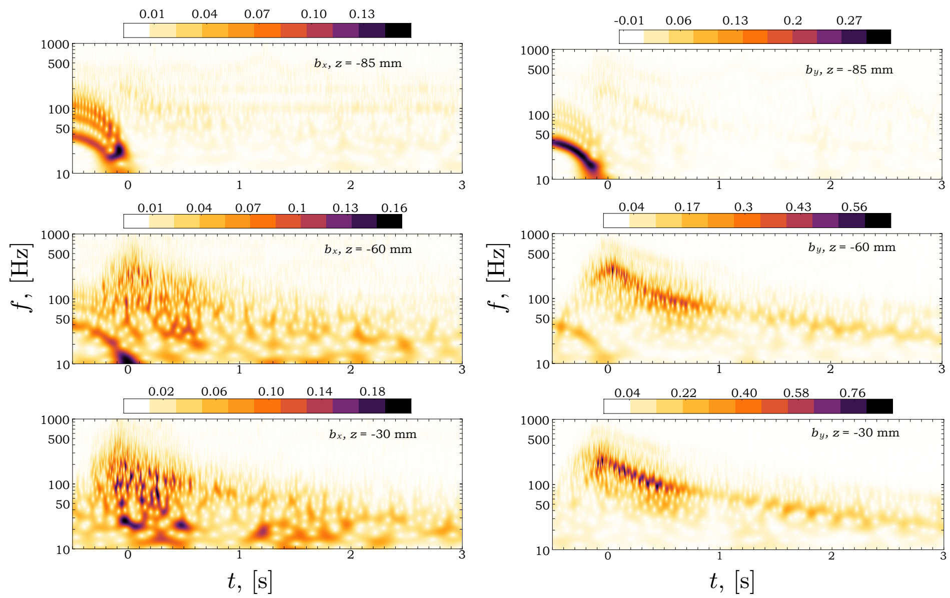

Fig. 7. Wavelet spectrograms of B_x (left) and B_y (right) fluctuations measured by the local probe at different positions: $z = -85$ mm (top), $z = -60$ mm (middle) and $z = -30$ mm (bottom).

field is measured in the central part of the channel cross-section and the velocity probe is localized in the vicinity of the wall at the opposite torus cross-section. Thus, no direct correlation between the measured signals can be expected, but it can be concluded that the behavior of the magnetic field generally follows the behavior of the poloidal velocity mode. Also, it should be noted that the magnetic field pulsations exhibit some secondary burst at $t \approx 1.5$ s, which is absent in the velocity measurements made in the wall layer.

Wavelet spectrograms shown in Fig. 6 and Fig. 7 provide a detailed presentation of the evolution of turbulent pulsations of velocity and magnetic field. One can see a burst of high frequency pulsations during the breaking and their decay attended by the shift of excited frequencies into the low frequency range, which is caused by the decay of the mean toroidal velocity. The dark arc in the left lower corner of the magnetic field spectrograms reflects the Earth magnetic field, which is recorded as an oscillating field in the rotating channel before the stop.

Another feature that attracts attention in the wavelet spectrogram of poloidal velocity is the strip going down from the frequency about 200 Hz at $t = 0$ to the frequency about 20 Hz at $t = 3$ s. It is worth to note that nothing similar has been observed in the velocity spectrograms recorded in the same channel, but *without* any tube inside it [5]. This strip is much better pronounced in the wavelet spectrogram of the radial component of magnetic field B_y in the central part of the channel (Fig. 7, right).

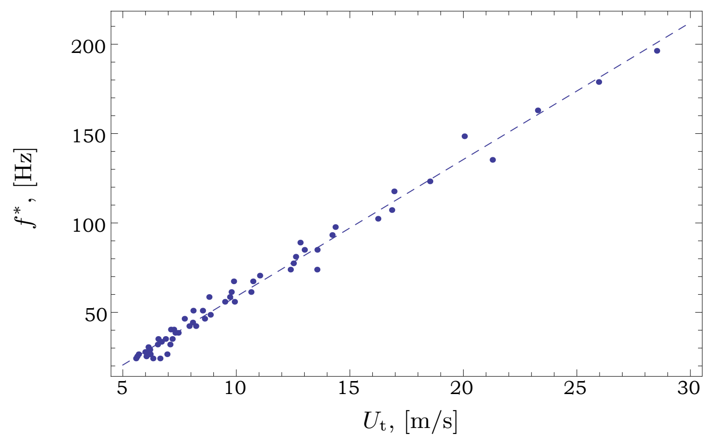

Fig. 8. Repetition rate of von Karman's vortices versus toroidal velocity. The linear fit gives the Strouhal number $\mathrm{St} = (7.6 \pm 0.2) \cdot 10^{-2}$.

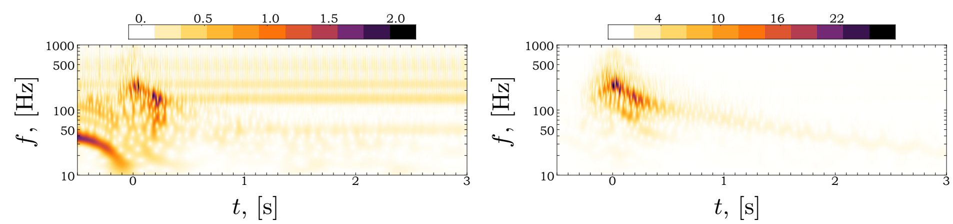

Fig. 9. Wavelet spectrograms of the half-sum (left) and half-difference (right) of magnetic flux fluctuations in two coils.

We explain this strip as a trace of von Karman's vortices generated by the stream flows around the tube installed in the channel. These vortices produce specific oscillations with a frequency defined by the ratio of the mean flow velocity U to the diameter d of the tube, $f = \mathrm{St} \cdot U/d$, where St is the Strouhal number [7]. Fig. 8 illustrates the dependence of the dominant frequency in the strip on the mean velocity. The linear fit of this plot gives an estimation for the Strouhal number $\mathrm{St} = (7.6 \pm 0.2) \cdot 10^{-2}$. It is considerably lower than the typical value 0.2. This difference can be explained by peculiarities of the flow: the flow is non-stationary (rapidly damping), strongly curved and circulating (the vortices do not vanish during one turnover).

The effect of von Karman's vortices manifests itself in the variations of the magnetic flux in two coils embracing the two halves of the cross-section. Measurements of the electromotive force in two coils make it possible to observe alternative pulsations of the averaged magnetic field over the channel half cross-sections. The total magnetic flux through both coils is practically constant – only weak noise occurs in the spectrogram shown in the left panel of Fig. 9. The spectrogram of the half-difference (right panel in the same figure) again reveals the strip provided by von Karman's vortices.

Thus, the measurement of the magnetic flux variations in two half-coils confirms the conservation of the total magnetic flux of the toroidal magnetic field (accurate within few percents). We verify the conservation of the total magnetic flux (in order to exclude any magnetic field generation inside the channel) by measuring the e.m.f. in the coil wound around the whole channel in parallel to the power coil. This measurement confirms the conservation of the total flux with an accuracy below 0.1%. However, the measurement of the magnetic field along the tube shows some decrease of the applied field only. This means that the magnetic field is partially displaced to the channel periphery in the y-direction, where the B_z field should increase. Apart from turbulent diamagnetism, the advection of the magnetic field partly frozen in the fluid can be caused by the flow around the tube. We have estimated the contribution of this drift by numerical simulations which gave the upper limit of the magnetic field drop in the tube, which is about 25% of the observed effect. Note that the magnetic Reynolds number defined through the radius of the tube and the toroidal velocity reaches about 0.7 only. This explains the weak effect of advection.

3. Discussion and conclusions. Experimental measurements of the induction effects in MHD flows caused by turbulence require significant efforts to provide a sufficient signal-to-noise ratio and special conditions for proper interpretation of contribution of different turbulent mechanisms. Only few studies have succeeded to single out a particular turbulent induction mechanism. So, the part of the α-effect based on the co-action of the large-scale vorticity and gradient of energy of turbulent pulsations was detected in the transient regime of the spin-down flow [8]. The experimental demonstration of the β-effect exploited precise measurements of the phase shift between the alternating applied and induced magnetic fields [3, 9]. The effect of turbulent diamagnetism was studied in [10, 11] by subtracting the contribution of the mean-velocity-induced field from the measured magnetic field. The mean-velocity-induced field was calculated numerically based on the velocity measurements made in a water prototype. However, the magnetic field induced by the mean flow was comparable with the fluctuation-driven magnetic field. Recently, in [12], a reduction of magnetic diffusivity in the turbulent flow has been found by solving a complicated inverse problem. All such experiments require thorough analysis. Direct observation of the turbulent e.m.f. estimated from simultaneous measurements of velocity and magnetic field pulsations by adjacent probes has been performed in Madison liquid sodium experiment [13]. This is indeed the most straightforward way to indicate the turbulent effect. However, the way of how to identify the contributions of the α- and β-effects is not clear in the case of the non-uniform mean magnetic field.

In this paper, we present an attempt of experimental study of the effect of magnetic field expulsion from the turbulent core of the flow. Our measurements show that at the highly turbulent stage of flow evolution the mean magnetic field is reduced by a factor of 0.7. Our claim can be substantiated with the help of the mean field theory. The effect of turbulent diamagnetism is predicted for inhomogeneous background turbulence as a contribution of the mean electromotive force

$$\mathscr{E} = -\gamma\, \mathbf{g} \times \mathbf{B}, \tag{1}$$

where $\mathbf{g} = u_{\mathrm{rms}}^{-2} \boldsymbol{\nabla}(u_{\mathrm{rms}}^2)$ is the normalized gradient of the energy of turbulent fluctuations and $\mathbf{B}$ is the mean magnetic field. The coefficient γ is determined by the statistical properties of the turbulent component of velocity. The effective advection of $\mathbf{B}$ can be considered as a result of the action of corresponding velocity $\mathbf{v}_d = -\gamma\mathbf{g}$. Reasonably assuming that the strongest gradient of turbulent energy is realized in the radial direction, we find a proper symmetry of experimental results with respect to the direction of the torus rotation. This requires additional efforts and assumptions f or quantitative arguments. Following [1], the turbulent transport coefficient can be evaluated as $\gamma \approx 0.1\mathrm{Rm}_{\mathrm{t}}^2\eta$, where η is the magnetic diffusivity and Rm_{t} is the turbulent magnetic Reynolds number. A precise estimate of Rm_{t} is hardly possible with the flow measurement which was made by one probe near the wall of the channel. Since the order of magnitude remains uncertain, we expect $\mathrm{Rm}_{\mathrm{t}} \approx 0.25 \div 2.5$. This gives an estimate $\gamma = (5 \cdot 10^{-4} \div 5 \cdot 10^{-2})\mathrm{m}^2/\mathrm{s}$. The absolute value of the vector **g** varies in the range from 10 to 100 m^{-1} depending on the profile of the turbulent energy. The upper estimate proves to be rather relevant for the boundary layer. So for the peak values one can expect an effective magnetic Reynolds number $\mathrm{Rm}_d = v_d r_0/\eta \approx 1$, which corresponds to the measured effect.

Acknowledgements. We thank the referee for useful comments and detailed suggestions that have led to improvements of the manuscript. Financial support from RFBR-Ural project No. 14-01-96010a is gratefully acknowledged.

REFERENCES

[1] K.-H. Rädler and R. Stepanov. Mean electromotive force due to turbulence of a conducting fluid in the presence of mean flow. *Phys. Rev. E*, vol. 73 (2006), no. 5, p. 056311.

[2] F. Stefani, A. Gailitis, and G. Gerbeth. Magnetohydrodynamic experiments on cosmic magnetic fields. *Zamm-Zeitschrift Fur Angewandte Mathematik Und Mechanik*, vol. 88 (2008), no. 12, pp. 930–954.

[3] P. Frick, V. Noskov, S. Denisov, and R. Stepanov. Direct Measurement of Effective Magnetic Diffusivity in Turbulent Flow of Liquid Sodium. *Phys. Rev. Lett.*, vol. 105 (2010), no. 18, pp. 184502–+.

[4] V. Noskov, *et al.* Dynamics of a turbulent spin-down flow inside a torus. *Phys. Fluids*, vol. 21 (2009), no. 4, pp. 045108–+.

[5] V. Noskov, S. Denisov, R. Stepanov, and P. Frick. Turbulent viscosity and turbulent magnetic diffusivity in a decaying spin-down flow of liquid sodium. *Phys. Rev. E*, vol. 85 (2012), no. 1, p. 016303.

[6] A. Gailitis, *et al.* The Riga dynamo experiment. *Surveys in Geophysics*, vol. 24 (2003), no. 3, pp. 247–267.

[7] L. Landau and E. Lifshitz. *Hydrodynamics* (M.: Nauka, in Russia, 1986).

[8] R. Stepanov, *et al.* Induction, helicity, and alpha effect in a toroidal screw flow of liquid gallium. *Phys. Rev. E*, vol. 73 (2006), no. 4, pp. 046310–+.

[9] S.A. Denisov, V.I. Noskov, R.A. Stepanov, and P.G. Frick. Measurements of turbulent magnetic diffusivity in a liquid-gallium flow. *JETP Lett.*, vol. 88 (2008), pp. 167–171.

[10] E.J. Spence, *et al.* Observation of a Turbulence-Induced Large Scale Magnetic Field. *Phys. Rev. Lett.*, vol. 96 (2006), no. 5, pp. 055002–+.

[11] E.J. Spence, *et al.* Turbulent Diamagnetism in Flowing Liquid Sodium. *Phys. Rev. Lett.*, vol. 98 (2007), no. 16, pp. 164503–+.

[12] S. Cabanes, N. Schaeffer, and H.-C. Nataf. Turbulence Reduces Magnetic Diffusivity in a Liquid Sodium Experiment. *Physical Review Letters*, vol. 113 (2014), no. 18, p. 184501.

[13] K. Rahbarnia, *et al.* Direct Observation of the Turbulent emf and Transport of Magnetic Field in a Liquid Sodium Experiment. *Astrophys. J.*, vol. 759 (2012), p. 80.

Received 16.12.2014